Nano Trends 11 (2025) 100132

Contents lists available at ScienceDirect

Nano Trends

journal homepage: www.elsevier.com/locate/nantre

Monitoring nanoparticle self-assembly on liquid subphases in situ in a vertical scattering geometry

Felix Lehmkühler [a,b,**], Fabian Westermeier [a], Juan J. Barrios-Capuchino [c], Daniel Weschke [a], Francesco Dallari [a,d], Wojciech Roseker [a], Wolfgang J. Parak [b,c], Florian Schulz [c,*]

[a] Deutsches Elektronen-Synchrotron DESY, 22607 Hamburg, Germany
[b] The Hamburg Centre for Ultrafast Imaging, Hamburg, Germany
[c] Institute of Nanostructure and Solid State Physics, Universität Hamburg, 22761 Hamburg, Germany
[d] Present address: Department of Physics and Astronomy, University of Padova, 35122 Padova, Italy

ARTICLE INFO

Keywords:
Self-assembly
Small-angle X-ray scattering
Synchrotron
Nanoparticles
Supercrystals

ABSTRACT

Nanoparticle (NP) self-assembly is a promising tool for the straightforward preparation of complex materials without lithography. Self-assembly on liquid subphases is established for the preparation of thin NP films with quasicrystalline order on large scales. Small-angle X-ray scattering (SAXS) at synchrotron radiation sources is in particular advantageous to study self-assembly in situ, providing detailed structural information with high temporal resolution. Here we present a new experimental setup that allows measuring SAXS in a vertical geometry. This way it is possible to study the self-assembly of nanoparticles on liquid subphases in situ as demonstrated with gold nanoparticles. In contrast to measurements with grazing incidence (GISAXS), spatial resolution in the μm range and sampling of the volume material is possible. Integration of optical microscopy allows observing the measurement position and formation of supercrystal flakes. The setup can be used to study self-assembly of various nanoparticles on liquid subphases but is not limited to such studies. It was realized at the beamline P10 at PETRA III (Deutsches Elektronen-Synchrotron DESY, Hamburg, Germany).

Introduction

Within the past decades, nanoparticle (NP) self-assembly has emerged as a powerful tool for the preparation of complex nanomaterials [1,2]. NPs of various materials and in different sizes and shapes can be assembled and the structure of the resulting materials can be tailored by judicious choice of the coating ligand. Interesting magnetic, electronic and optical properties are aimed for, especially new emerging properties resulting from strong and coherent collective coupling in the material [3–5]. Inspired by the Langmuir-Blodgett technique, self-assembly of NP on liquid subphases has been tested to prepare monolayer films [6]. Two immiscible solvents are used in this method, one containing the material that is to be assembled. Typically, a dispersion of the nanomaterial in an apolar organic solvent like toluene, hexane or heptane slowly evaporates on top of a polar subphase (e.g. water, ethylene or diethylene glycol (EG or DEG), acetonitrile). After complete evaporation, the self-assembled material remains floating on the liquid subphase and can be then transferred to arbitrary substrates for further treatment or experiments. Various crystalline superstructures have been demonstrated, including binary structures [7,8], large-scale monolayer films [9,10], defined crystals from very small nanoclusters (diameter, $d \sim 1$ nm) [11] as well as from large plasmonic gold NP (AuNP) [12]. These are just a few examples from the broad range of intriguing structures that have been demonstrated and we refer to available reviews for a more detailed overview and discussion [1,3,13–19]. Because self-assembly is a complex process involving various forces and interactions, in situ studies are highly desirable and valuable for the informed development and optimization of robust protocols for the reproducible and controlled preparation of functional materials. The most common techniques used to this end are electron microscopy and small-angle X-ray scattering- (SAXS-) based approaches and a recent overview and discussion of these approaches in the context of NP

* Corresponding author.
** Corresponding author at: Deutsches Elektronen-Synchrotron DESY, 22607 Hamburg, Germany.
E-mail addresses: felix.lehmkuehler@desy.de (F. Lehmkühler), florian.schulz@physik.uni-hamburg.de (F. Schulz).

https://doi.org/10.1016/j.nwnano.2025.100132
Received 30 March 2025; Received in revised form 24 July 2025; Accepted 24 July 2025
Available online 6 August 2025
2666-9781/© 2025 The Author(s). Published by Elsevier Ltd. This is an open access article under the CC BY license (http://creativecommons.org/licenses/by/4.0/).

self-assembly is available [3]. Liquid-cell-TEM approaches have revealed valuable information about crystallization mechanisms, but also confirmed that the self-assembly process and outcome is affected by the experimental conditions (in particular charging effects due to the electron beam), which is a well-known effect for this approach [20]. SAXS provides the unique advantage of measuring in conditions similar to laboratory, at ambient pressure and in the according geometry. SAXS in transmission (in contrast to GISAXS) has several advantages, in particular it allows a much higher spatial resolution, but is not possible in situ with the common horizontal geometry at synchrotron radiation sources [21,22]. Here, we present a vertical geometry for in situ SAXS measurements of NP self-assembly on liquid subphases at beamline P10 of PETRA III (Deutsches Elektronen-Synchrotron DESY, Hamburg, Germany), based on a six-circle diffractometer setup. The setup was successfully tested with AuNP, but can be used to study the whole range of nanomaterials in terms of size, shape and material/composition that is typically studied in this context.

Experimental section

Materials. Tetrachloroauric(III) acid (≥ 99.9 % trace metals basis), hexadecyltrimethylammonium bromide (CTAB, ≥ 98 %) and chloride (CTAC, ≥98 %), L-ascorbic acid (reagent grade), and sodium borohydride (≥ 98 %) were obtained from Sigma-Aldrich (USA). Toluene (≥ 99.5 %), tetrahydrofuran (≥99.5 %), and ethanol (denat., > 96 %) were purchased from VWR (USA). Diethylene glycol (DEG, reagent grade) was obtained from Merck (Germany). Thiolated polystyrene (PSSH: M_n = 5300 g/mol, M_w = 5800 g/mol) was obtained from Polymer Source (Canada). All reagents were used without further treatment.

AuNP Synthesis, Functionalization, and Self-Assembly. CTAC stabilized AuNPs with a low dispersity were synthesized with a slightly modified version of the protocol presented by Zheng et al. [23] and coated with PSSH ligands as described previously [12,24]. The self-assembly took place on the liquid subphase, DEG, by pipetting 150 µL of the AuNP@PSSH dispersion in toluene onto the subphase (200 µL) in the assembled sample cell.

Coherent X-ray scattering experiments. The in situ SAXS experiments were conducted at the beamline P10 at PETRA III (Deutsches Elektronen-Synchrotron DESY, Hamburg, Germany). A two-mirror system was used for higher harmonics rejection. The experimental setup and the measurements are described and discussed in detail in the main text. For the optical microscopy, a live video microscopy (LVM) system with a working distance of 108 mm and equipped with a high-resolution color camera was used (Hinze-Optoengineering, Braunschweig, Germany). Optical illumination of the sample cell from below was realized with LED-lamps placed close to the sample cell.

Cleaning of the sample cell. The sample cell was disassembled by carefully removing the Si_3N_4 window with tweezers and cleaned with toluene in a fumehood. If necessary, further cleaning with aqua regia was used to quantitatively remove all gold deposits. *[Caution! Aqua regia is highly corrosive and releases toxic gases. It must be prepared and handled only by trained personnel in a well-ventilated fume hood while wearing appropriate personal protective equipment. All procedures must comply with relevant institutional safety protocols and local regulations regarding chemical handling and waste disposal.]*.

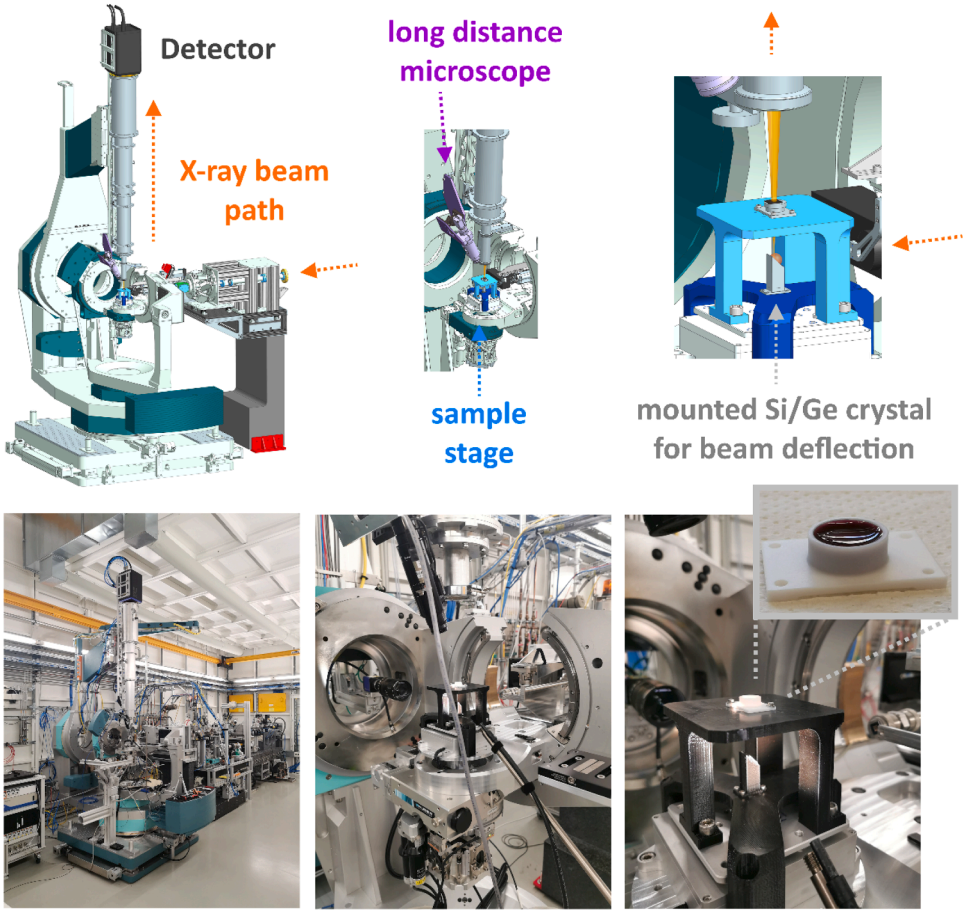

Fig. 1. Experimental setup at the beamline P10 of PETRA III based on a six-circle diffractometer setup. Top row: Renderings of the model, bottom row: Photos, from the left to the right a zoom towards the sample cell is displayed.

Results

Fig. 1 shows a scheme of the experiment located at the beamline P10 at PETRA III (Deutsches Elektronen-Synchrotron DESY, Hamburg, Germany). Based on a six-circle diffractometer (HUBER Diffraktionstechnik GmbH & Co. KG, Rimsting, Germany) setup, we used a germanium crystal to deflect the beam (8.052 keV) at the (333) plane by 90° upwards. At different photon energies other planes or crystals may be used (Si(333) at 8.388 keV; Si(555) at 13.980 keV). The Germanium crystal was placed in the center of rotation of the diffractometer. Placed on xyz-translation stages the crystal features 3 translational and 3 rotational degrees of freedom, allowing thus for the precise alignment of the crystal with respect to the beam and upward pointing direction. Approximately 36 mm above the crystal, the sample cell was positioned on a heavy load xyz-translational piezo stage (SmarAct GmbH, Oldenburg, Germany). This translational stage was moving independent of the Germanium crystal translations, allowing thus for easy scanning of the sample in the x-ray beam. Please note that due to the liquid nature of the sample, the sample surface is always aligned in the horizontal plane. The sample cell was milled from Teflon and a detailed sketch is provided as Supporting Information (Supporting Figure S1). At the bottom, a square silicon nitride window (3 mm x 3 mm, 1000 nm thickness) in a square silicon support frame (7.5 mm x 7.5 mm, 525 μm thickness, Silson, UK) was carefully placed into the according indentation. The liquid subphase (diethylene glycol, DEG) was pipetted on top. In our experiments we observed no leakage of the DEG even without any further fixing of the silicon nitride window. However, when water is desired as a subphase, additional measures to seal the bottom of the cell might be necessary. In case of damage or contamination of the SiN window it can be easily removed for replacement or cleaning. Because the chemically very stable Teflon is used as a material for the sample cell, cleaning is straightforward. In our case toluene was used for cleaning. Resistant adhesions of AuNP were removed with aqua regia (see Methods). The sample cell was covered with polyimide foil (poly(4,4′-oxydiphenylene-pyromellitimide, Kapton®, DuPont, US) in case a slowed evaporation was desired.

Above the sample cell an evacuated flight tube was positioned (length: 1.60 m) and an Eiger X4M detector was placed at the end of it. The sample-detector distance was 1784 mm. On the side of the flight tube, an optical microscope with a long working distance (108 mm) was attached. Beryllium compound refractive lenses were used to focus the x-rays on the sample plane. An additional pinhole of 100 μm diameter was placed between germanium crystal and sample to reduce parasitic scattering. After alignment, the x-ray spot size on the sample was 2.5 μm x 4.5 μm (perpendicular and parallel to the original beam direction). In a typical experiment we did not move the stage throughout the self-assembly to avoid additional agitation of the sample.

Polystyrene-coated AuNP, AuNP@PSSH, in toluene have been shown to assemble into well-defined layered 2D-hexagonal supercrystalline thin-films on DEG [12]. The size and spacing of the AuNP in the structures can be tuned, for instance to maximize the light-matter coupling in the supercrystals with interesting physical consequences [25,26]. We have performed ex situ experiments with coherent SAXS on such supercrystals previously, revealing domain sizes and orientations, thickness-dependent features and thickness-independent degree of sixfold order [27]. Up to now, however, the thickness (number of layers) of the supercrystals and domain sizes cannot be perfectly controlled. To gain a better understanding of the self-assembly of these AuNP@PSSH we used them as the first model system in the new setup for in situ studies. Fig. 2 shows the SAXS curves for AuNP with 40 nm diameter. Thin-film supercrystals floating on the liquid subphase are formed during the evaporation of the toluene. Selected curves reveal the onset of Bragg reflections during the self-assembly. The sample was not moved via the piezo stage during the experiment, but it is important to keep in mind that the forming supercrystal fragments are freely floating on the liquid subphase, i.e. the beam does not necessarily sample the exact

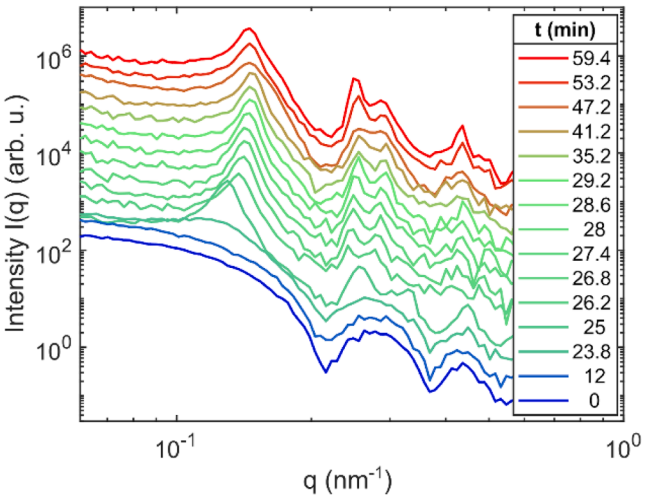

Fig. 2. SAXS data obtained during the crystallization of AuNP (40 nm diameter) on the liquid subphase. Indication of crystallization (or motion of crystallites into the beam) can be observed after about 25 min.

same position of the according supercrystal fragment throughout the experiment. For the interpretation, the correlated optical microscopy data is therefore valuable. Because the AuNP are comparably large, even small crystallites and agglomerates of AuNP can be clearly discerned. From the optical microscopy monitoring it is evident that under the experimental conditions the kinetics of self-assembly were highly heterogeneous. The first observable crystallites formed within minutes but nucleation of new crystallites was observed throughout the experiment. Another important observation from the optical microscopy is the presence of strong convective flows and occasional stress-induced rapid movements and rearrangements in the sample. As a tendency with increasing crystallite size these movements are reduced to a minimum and a continuous growth at the edges of the crystallites takes place. In this stage, even the mass transport and density gradients can be observed, again pointing at a dynamically and spatially heterogeneous process. An exemplary optical microscopy image capturing different phases of the assembly is provided as Supporting Information (Figure S2). Turbulences and flows can be significantly reduced by covering the sample cell, thus slowing down the evaporation of the solvent and avoiding external disturbances. The fluid dynamics in the sample are to some extent intrinsic and cannot be completely avoided. The meniscus of the toluene in the sample cell is concave, in the center of the sample cell the toluene layer is the thinnest and accordingly completely evaporated first. Therefore, the first nucleation of crystallites could be expected to take place in the center. Similar to the well-known coffee ring effect, the different evaporation rates at different positions of the sample cell can lead to convective flows within the toluene and according mass transport towards the center. In the optimum case, a large crystalline flake could therefore grow in the center, but due to fluctuations in mass transport and convection the thickness is not always uniform and voids can be included. These observations just from optical microscopy already provide some guidelines for optimization of the process.

To gain a more detailed view on the structures forming during self-assembly, the structure factors were calculated by dividing the experimental $I(q)$ by the form factor $F(q)$ of the dispersed AuNP@PSSH (Supporting Information, Figure S3). Note that the continuous densification of the superlattice (formed by the assembling AuNP@PSSH) due to the evaporation of the solvent leads to a gradual increase of multiple scattering that has to be considered [28]. The main contribution of multiple scattering can be observed at the form factor minima that smear out with increasing concentration. In consequence, this may be misinterpreted as additional peaks in the structure factor. The resulting

structure factors are shown in Fig. 3 for selected times before, during and after the assembly. We also added the results after 116.5 min and 142.9 min which represent final states of the formed structures. After around 24 min a broad peak appears around 0.13 nm^{-1} whose amplitude grows quickly in the following. Also, its position changes towards larger q and further peaks appear. The peaks labeled with q1, q3 and q4 correspond to a 2D hexagonal lattice, also reported before as the final state of the assembly of such particles [12,27]. During early times of the assembly, we find a shoulder around q2. This can be associated with the (11) reflection of a 2D cubic lattice. As this shoulder disappears at longer times, the cubic state appears as an intermediate structure during the assembly. Note that if we do not account for multiple scattering with a correction, a clear peak shows up at q2 (Supporting Information, Figure S4). This artifact originates from the smeared-out particle form factor minima at higher concentrations and can thus be misinterpreted as a coexisting phase, in our case almost matching a bcc structure.

The correlated SAXS-optical microscopy data confirm that the formation of the first agglomerates or crystallites already takes places within the initial phase of the experiment (i.e. within the first minutes for fast evaporation (no cover on the sample cell) or within the first 30 min for slower evaporation (sample cell covered with Kapton®). The initial lattice constant of the crystallites in this run was roughly $a = 57$ nm. After densification of the lattice, it was reduced to $a = 49.2$ nm, which corresponds to an average gap of 7.8 nm between neighboring particles. The timescale of the densification is visualized in Fig. 4 where an exponential fit to the experimental data reveals a characteristic time scale of ~ 2 min. In the final dried state, the thin-film supercrystal was large enough to remain unaffected by motor movements and could be reliably mapped. Fig. 4 shows the distribution of lattice constants in this state, derived from the mapping data, indicating a slight additional decrease in the lattice constant. due to final drying.

The mapping data of the final dried state also reveal the very narrow distribution of lattice constants with a full width at half maximum of 0.25 nm and a standard deviation of 0.1 nm. This observation underlines the well-defined crystallinity of the thin-film supercrystals in accordance with our previous studies [12,27].

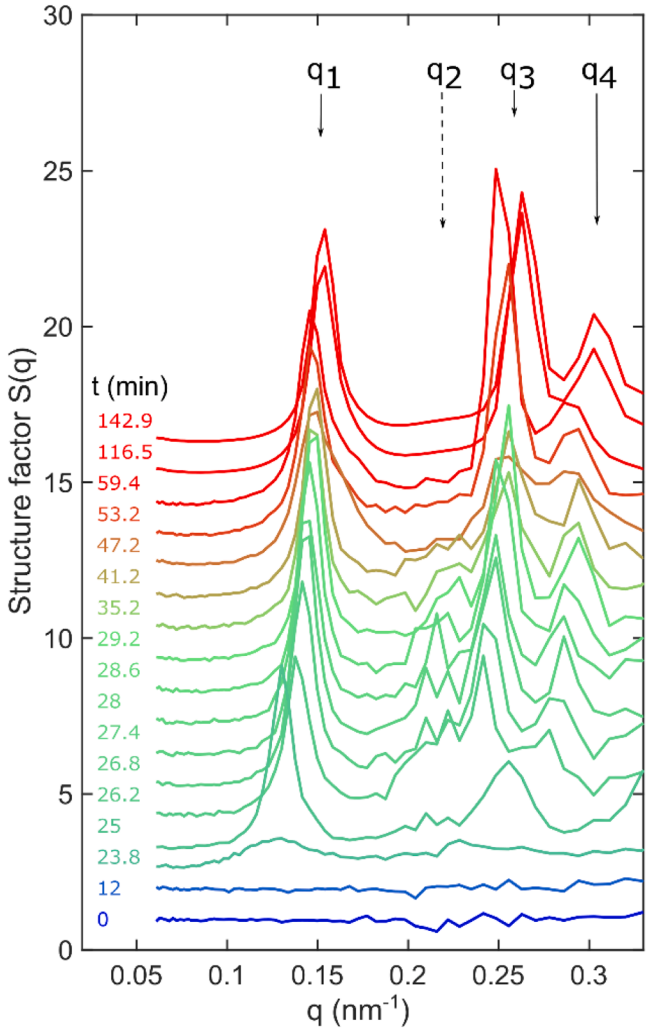

Fig. 3. Structure factors S(q) for several experimental times. Data is shifted vertically for clarity. The labels q1, q3 and q4 describe the (10), (11), and (20) reflection of a 2D hexagonal lattice. Around q2 = 0.22 nm^{-1} a shoulder appears at the beginning of the assembly. This corresponds to the 2D cubic (11) reflection.

Discussion

To present and discuss the newly developed experimental setup, we focused herein on a simple and established model system: the supercrystal formation by spherical AuNP@PSSH. The advantage of this model system is the formation of highly defined supercrystals with a narrow distribution of lattice constants in the final state. The AuNP cores with a diameter of 40 nm scatter and absorb strongly, which benefits the confident analysis of experimental data, because it allows for in-situ monitoring of supercrystal formation with optical microscopy. Compared to electron microscopy studies, the advantages of SAXS measurements include robust statistics of the high-resolution structural data and the possibility of measuring under laboratory-like conditions. Compared to GISAXS experiments the vertical scattering geometry allows for small footprints of the beam, resulting in higher spatial resolution, and volume sampling of the material. The reproducibility of the experiment strongly depends on the sample system. Spherical AuNP@PSSH are known to form homogeneous 2D-hexagonal thin-film supercrystals reproducibly under the given experimental conditions [24], but more complex samples, such as binary mixtures or differently shaped NP, may lead to a larger variety of crystalline phases and less reproducibility of the self-assembly experiments [29]. In such cases more measurements and control experiments may be required. We focused here on the self-assembly on a liquid subphase with a specific, well-defined model system, but the utility of the vertical scattering geometry is not limited to such experiments. The requirements for the samples are their scattering strength ensuring sufficient intensity for meaningful SAXS measurements. If this requirement is fulfilled, there is no principal limitation regarding material, shape and structure of the sample. For instance, also complex core-shell materials, AuNP obtained by different synthetic approaches, different materials and shapes, and other processes than NP self-assembly can also be studied, such as crystallization and aggregation processes [30–42].

Conclusion

In summary, we presented a new experimental setup for SAXS measurements in a vertical scattering geometry that allows in situ measurements of NP self-assembly on a liquid subphase. We demonstrated its potential using spherical AuNP as a simple model system. We observed the formation and densification of the AuNP superlattice and characterized the final dried state. In-situ data of structure formation under laboratory-like conditions (ambient pressure and temperature) are hard to obtain with other methods. The setup can be applied to monitor the formation of more complex supercrystals in future studies. Open challenges include the optimization of motor movements to allow accurate positioning and in situ mapping experiments without inducing movements of the crystallites on the liquid subphase. This applies in particular for the early stage of the experiments, the larger crystallites in the final stage were much less affected. The experimental approach allows to obtain valuable in situ data of self-assembly on a liquid-subphase

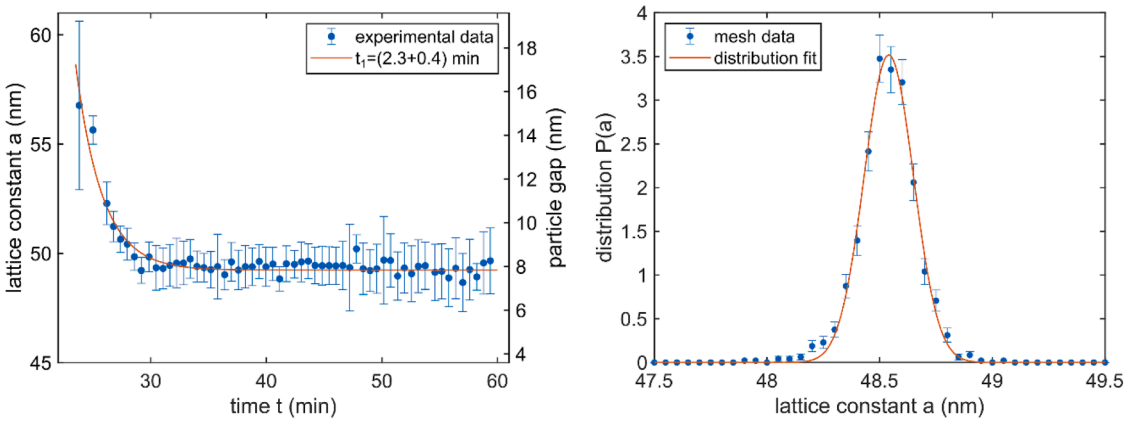

Fig. 4. Left: Change of lattice constant over time during the self-assembly experiment. The data was fitted by an exponential resulting in a characteristic time scale of 2.3 min. Right: Distribution of lattice constants in the final dried state. The mean lattice constant is (48.5 ± 0.1) nm, slightly smaller than the final state (49.2 nm) in the in-situ measurements, indicating a slight additional densification in the drying process. The error bars of the lattice constants are obtained by error propagation of the fitted peak positions in $S(q)$. To this end, the peaks of the individual $S(q)$ measurements are modelled within the corresponding q bins by a Gaussian. As the first peak around 0.15 nm^{-1} is present since the onset of structure formation, the lattice constants can be directly obtained from the peak positions. The error of the lattice constant is then the error propagation of the error of the fitted peak position. The other peaks are then used as control measures.

but is not limited to such experiments. Crystallization directly on the Si_3N_4 windows, i.e. without a liquid subphase, might be monitored as well. This will advance our understanding of NP self-assembly using well-established synthesis methods for high-quality supercrystals - an emerging class of new functional materials.

CRediT authorship contribution statement

Felix Lehmkühler: Writing – review & editing, Writing – original draft, Visualization, Supervision, Resources, Project administration, Investigation, Funding acquisition, Formal analysis, Data curation, Conceptualization. **Fabian Westermeier:** Writing – review & editing, Writing – original draft, Visualization, Resources, Investigation, Funding acquisition, Formal analysis, Data curation, Conceptualization. **Juan J. Barrios-Capuchino:** Writing – review & editing, Investigation. **Daniel Weschke:** Writing – review & editing, Writing – original draft, Visualization, Investigation, Data curation, Conceptualization. **Francesco Dallari:** Writing – review & editing, Investigation, Formal analysis. **Wojciech Roseker:** Writing – review & editing, Visualization, Investigation, Formal analysis, Data curation. **Wolfgang J. Parak:** Writing – review & editing, Supervision, Resources. **Florian Schulz:** Writing – review & editing, Writing – original draft, Visualization, Supervision, Resources, Project administration, Investigation, Funding acquisition, Formal analysis, Conceptualization.

Declaration of competing interest

The authors declare no conflict of interest.

Acknowledgements

All authors thank the PIER Idea Fund - Hamburg for funding of the project under PIF-2021-02.

JBC was funded by a PhD fellowship (862535) from the Mexican National Council for Science and Technology (CONACYT). Parts of this work were supported by the Cluster of Excellence 'Advanced Imaging of Matter' of the Deutsche Forschungsgemeinschaft (DFG) - EXC 2056 - project ID 3907159948 (WJP). The authors acknowledge DESY (Hamburg, Germany), a member of the Helmholtz Association HGF, for the provision of experimental facilities. This research project was carried out at PETRA III. Beamtime was allocated for proposals I-20211357 and I-20221388. This research was supported, in part, through the Maxwell computational resources operated at Deutsches Elektronen-Synchrotron DESY, Hamburg, Germany. We acknowledge financial support from the Open Access Publication Fund of Universität Hamburg.

Supplementary materials

Supplementary material associated with this article can be found, in the online version, at doi:10.1016/j.nwnano.2025.100132.

References

[1] M.A. Boles, M. Engel, D.V. Talapin, Self-assembly of colloidal nanocrystals: from intricate structures to functional materials, Chem. Rev. 116 (2016) 11220–11289, https://doi.org/10.1021/acs.chemrev.6b00196.
[2] K.J.M. Bishop, C.E. Wilmer, S. Soh, B.A. Grzybowski, Nanoscale Forces and Their Uses in Self-Assembly, Small 5 (2009) 1600, https://doi.org/10.1002/smll.200900358.
[3] F. Schulz, I. Lokteva, W.J. Parak, F. Lehmkühler, Recent notable approaches to study self-assembly of nanoparticles with X-ray scattering and electron microscopy, Part. Part. Syst. Charact. 38 (2021) 2100087, https://doi.org/10.1002/ppsc.202100087.
[4] K.S. Sugi, A. Maier, M. Scheele, Emergent properties in supercrystals of atomically precise nanoclusters and colloidal nanocrystals, Chem. Commun. 58 (2022) 6998–7017, https://doi.org/10.1039/D2CC00778A.
[5] D.V. Talapin, M. Engel, P.V. Braun, Functional materials and devices by self-assembly, MRS Bull. 45 (2020) 799–806, https://doi.org/10.1557/mrs.2020.252.
[6] V. Aleksandrovic, D. Greshnykh, I. Randjelovic, A. Frömsdorf, A. Kornowski, S. V. Roth, C. Klinke, H. Weller, Preparation and electrical properties of cobalt–Platinum nanoparticle monolayers deposited by the Langmuir–Blodgett technique, ACS Nano 2 (2008) 1123, https://doi.org/10.1021/nn800147a.
[7] A. Dong, J. Chen, P.M. Vora, J.M. Kikkawa, C.B. Murray, Binary nanocrystal superlattice membranes self-assembled at the liquid–air interface, Nature 466 (2010) 474–477, https://doi.org/10.1038/nature09188.
[8] X. Ye, C. Zhu, P. Ercius, S.N. Raja, B. He, M.R. Jones, M.R. Hauwiller, Y. Liu, T. Xu, A.P. Alivisatos, Structural diversity in binary superlattices self-assembled from polymer-grafted nanocrystals, Nat. Commun. 6 (2015) 10052, https://doi.org/10.1038/ncomms10052.
[9] T. Wen, S.A. Majetich, Ultra-large-area self-assembled monolayers of nanoparticles, ACS Nano 5 (2011) 8868, https://doi.org/10.1021/nn2037048.
[10] K. Wang, H. Ling, Y. Bao, M. Yang, Y. Yang, M. Hussain, H. Wang, L. Zhang, L. Xie, M. Yi, W. Huang, X. Xie, J. Zhu, A centimeter-scale inorganic nanoparticle superlattice monolayer with non-close-packing and its high performance in memory devices, Adv. Mater. 30 (2018) 1800595, https://doi.org/10.1002/adma.201800595.
[11] F. Fetzer, A. Maier, M. Hodas, O. Geladari, K. Braun, A.J. Meixner, F. Schreiber, A. Schnepf, M. Scheele, Structural order enhances charge carrier transport in self-assembled Au-nanoclusters, Nat. Commun. 11 (2020) 6188, https://doi.org/10.1038/s41467-020-19461-x.
[12] Florian Schulz, Ondřej Pavelka, Felix Lehmkühler, Fabian Westermeier, Yu Okamura, Niclas S. Mueller, Stephanie Reich, Holger Lange, Structural order in plasmonic superlattices, Nat. Commun. 11 (2020) 3821, https://doi.org/10.1038/s41467-020-17632-4.
[13] K.J. Si, Y. Chen, Q. Shi, W. Cheng, Nanoparticle superlattices: the roles of soft ligands, Adv. Sci. 5 (2018) 1700179, https://doi.org/10.1002/advs.201700179.

[14] K. Deng, Z. Luo, L. Tan, Z. Quan, Self-assembly of anisotropic nanoparticles into functional superstructures, Chem. Soc. Rev. 49 (2020) 6002–6038, https://doi.org/10.1039/D0CS00541J.
[15] A. Klinkova, R.M. Choueiri, E. Kumacheva, Self-assembled plasmonic nanostructures, Chem. Soc. Rev. 43 (2014) 3976, https://doi.org/10.1039/C3CS60341E.
[16] P. van Rijn, M. Tutus, C. Kathrein, L. Zhu, M. Wessling, U. Schwaneberg, A. Böker, Challenges and advances in the field of self-assembled membranes, Chem. Soc. Rev. 42 (2013) 6578, https://doi.org/10.1039/C3CS60125K.
[17] L. Xu, W. Ma, L. Wang, C. Xu, H. Kuang, N.A. Kotov, Nanoparticle assemblies: dimensional transformation of nanomaterials and scalability, Chem. Soc. Rev. 42 (2013) 3114, https://doi.org/10.1039/C3CS35460A.
[18] C. Yi, Y. Yang, B. Liu, J. He, Z. Nie, Polymer-guided assembly of inorganic nanoparticles, Chem. Soc. Rev. 49 (2020) 465–508, https://doi.org/10.1039/C9CS00725C.
[19] Y. Yang, C. Gu, J. Li, Sub-5 nm metal nanogaps: physical properties, fabrication methods, and device applications, Small 15 (2019) 1804177, https://doi.org/10.1002/smll.201804177.
[20] Y. Zhong, V.R. Allen, J. Chen, Y. Wang, X. Ye, Multistep crystallization of dynamic nanoparticle superlattices in nonaqueous solutions, J. Am. Soc. Chem. 144 (2022) 14915–14922, https://doi.org/10.1021/jacs.2c06535.
[21] Irina Lokteva, Michael Koof, Michael Walther, Gerhard Grübel, Felix Lehmkühler, Monitoring nanocrystal self-assembly in real time using In situ small-angle X-ray scattering, Small 15 (2019) 1900438, https://doi.org/10.1002/smll.201900438.
[22] I. Lokteva, M. Walther, M. Koof, G. Grübel, F. Lehmkühler, In situ small-angle X-ray scattering environment for studying nanocrystal self-assembly upon controlled solvent evaporation, Rev. Sci. Instrum. 90 (2019) 36103, https://doi.org/10.1063/1.5082685.
[23] Y. Zheng, X. Zhong, Z. Li, Y. Xia, Successive, seed-mediated growth for the synthesis of single-crystal gold nanospheres with uniform diameters controlled in the range of 5–150 nm, Part. Part. Syst. Charact. 31 (2014) 266–273, https://doi.org/10.1002/ppsc.201300256.
[24] F. Schulz, H. Lange, Optimizing interparticle gaps in large-scale gold nanoparticle supercrystals for flexible light-matter coupling, Adv. Opt. Mater. 10 (2022) 2202064, https://doi.org/10.1002/adom.202202064.
[25] N.S. Mueller, E. Pfitzner, Y. Okamura, G. Gordeev, P. Kusch, H. Lange, J. Heberle, F. Schulz, S. Reich, Surface-enhanced raman scattering and Surface-enhanced infrared absorption by plasmon polaritons in three-dimensional nanoparticle supercrystals, ACS Nano (2021), https://doi.org/10.1021/acsnano.1c00352.
[26] N.S. Mueller, Y. Okamura, B.G.M. Vieira, S. Juergensen, H. Lange, E.B. Barros, F. Schulz, S. Reich, Deep strong light–matter coupling in plasmonic nanoparticle crystals, Nature 583 (2020) 780–784, https://doi.org/10.1038/s41586-020-2508-1.
[27] Florian Schulz, Fabian Westermeier, Francesco Dallari, Verena Markmann, Holger Lange, Gerhard Grübel, Felix Lehmkühler, Plasmonic supercrystals with a layered structure studied by a combined TEM-SAXS-XCCA approach, Adv. Mater. Interfaces 7 (2020) 2000919, https://doi.org/10.1002/admi.202000919.
[28] E.F. Semeraro, J. Möller, T. Narayanan, Multiple-scattering effects in SAXS and XPCS measurements in the ultra-small-angle region, J. Appl. Cryst. 51 (2018) 706–713, https://doi.org/10.1107/S160057671800417X.
[29] J. Marcone, S. Juergensen, J. Barrios-Capuchino, X. Li, C. Goldmann, A. Köppen, W. Pfeiffer, F. Lehmkühler, W.J. Parak, M. Kociak, M. Impéror-Clerc, S. Reich, C. Hamon, F. Schulz, Plasmonic polymorphs by combining shape anisotropy and soft interactions in bipyramid thin-films, Small (2025) 2500389, https://doi.org/10.1002/smll.202500389 n/a.
[30] X. Huang, J. Zhu, B. Ge, F. Gerdes, C. Klinke, Z. Wang, Situ constructing the kinetic roadmap of octahedral nanocrystal assembly toward controlled superlattice fabrication, J. Am. Soc. Chem. (2021), https://doi.org/10.1021/jacs.0c12087.
[31] D.K. Smith, B. Goodfellow, D.-M. Smilgies, B.A. Korgel, Self-assembled simple hexagonal AB2 binary nanocrystal superlattices: SEM, GISAXS, and defects, J. Am. Soc. Chem. 131 (2009) 3281, https://doi.org/10.1021/ja8085438.
[32] T. Paik, D.-K. Ko, T.R. Gordon, V. Doan-Nguyen, C.B. Murray, Studies of liquid crystalline self-assembly of GdF3 nanoplates by In-plane, out-of-plane SAXS, ACS Nano 5 (2011) 8322.
[33] Francesca Pietra, Freddy T. Rabouw, Wiel H. Evers, Dima V. Byelov, Andrei V. Petukhov, Celso de Mello Donegá, Daniël Vanmaekelbergh, Semiconductor nanorod self-assembly at the liquid/air interface studied by in situ GISAXS and ex situ TEM, Nano Lett. 12 (2012) 5515–5523, https://doi.org/10.1021/nl302360u.
[34] R. Buonsanti, T.E. Pick, N. Krins, T.J. Richardson, B.A. Helms, D.J. Milliron, Assembly of ligand-stripped nanocrystals into precisely controlled mesoporous architectures, Nano Lett. 12 (2012) 3872, https://doi.org/10.1021/nl302206s.
[35] A. Dong, Y. Jiao, D.J. Milliron, Electronically coupled nanocrystal superlattice films by in Situ Ligand exchange at the liquid–Air interface, ACS Nano 7 (2013) 10978, https://doi.org/10.1021/nn404566b.
[36] P. Born, A. Munoz, C. Cavelius, T. Kraus, Crystallization mechanisms in convective particle assembly, Langmuir 28 (2012) 8300, https://doi.org/10.1021/la2048618.
[37] Santanu Maiti, Alexander André, Rupak Banerjee, Jan Hagenlocher, Oleg Konovalov, Frank Schreiber, Marcus Scheele, Monitoring self-assembly and Ligand exchange of PbS nanocrystal superlattices at the liquid/air interface in real time, J. Phys. Chem. Lett. 9 (2018) 739–744, https://doi.org/10.1021/acs.jpclett.7b03278.
[38] Q. Guo, X. Teng, H. Yang, Fabrication of magnetic FePt patterns from Langmuir–Blodgett films of platinum–Iron oxide core–Shell nanoparticles, Adv. Mater. 16 (2004) 1337–1341, https://doi.org/10.1002/adma.200400596.
[39] L. Gentile, H. Mateos, A. Mallardi, M. Dell'Aglio, A. de Giacomo, N. Cioffi, G. Palazzo, Gold nanoparticles obtained by ns-pulsed laser ablation in liquids (ns-PLAL) are arranged in the form of fractal clusters, J. Nanopart. Res. 23 (2021) 35, https://doi.org/10.1007/s11051-021-05140-5.
[40] F.S. Abdulwahid, A.J. Haider, S. Al-Musawi, Effect of laser parameter on Fe3O4 NPs formation by pulsed laser ablation in liquid, AIP Conf. Proc. (2023) 2769, https://doi.org/10.1063/5.0129824.
[41] A.H.F. Alnasraui, I.H. Joe, S. Al-Musawi, Design and synthesize of folate decorated Fe3O4@Au-DEX-CP nano formulation for targeted drug delivery in colorectal cancer therapy: In vitro and in vivo studies, J. Drug. Deliv. Sci. Technol. 87 (2023) 104798, https://doi.org/10.1016/j.jddst.2023.104798.
[42] A.J. Haider, M.A. Al-Kinani, S. Al-Musawi, Preparation and characterization of gold coated super paramagnetic iron nanoparticle using pulsed laser ablation in liquid method, Key Eng. Mater. 886 (2021) 77–85, https://doi.org/10.4028/www.scientific.net/KEM.886.77.